Available online at www.sciencedirect.com
ScienceDirect
Journal of the European Ceramic Society 27 (2007) 2577–2589
www.elsevier.com/locate/jeurceramsoc

Influence of attrition milling on the electrical properties of undoped-$BaTiO_3$

O.P. Thakur [a,b], A. Feteira [a], B. Kundys [c], D.C. Sinclair [a,*]

[a] *Ceramics and Composites Laboratory, Department of Engineering Materials, University of Sheffield, Mappin Street, Sheffield S1 3JD, UK*
[b] *Electroceramics Division, Solid State Physics Laboratory, Timarpur, Delhi 110054, India*
[c] *Laboratoire CRISMAT, CNRS 6508, ENSICAEN, 6 Bd. Du Marechal Juin, 14050 Caen Cedex, France*

Received 20 July 2006; received in revised form 26 September 2006; accepted 7 October 2006
Available online 8 December 2006

Abstract

Undoped-$BaTiO_3$ powder prepared from the mixed oxide route (0 h sample) has been attrition milled using yttria-stabilized ZrO_2 milling media for 0.5–3 h prior to formation of dense ceramics. Both isovalent ($Zr^{4+} \rightarrow Ti^{4+}$) and aliovalent ($Y^{3+} \rightarrow Ba^{2+}$) dopant contamination effects have been observed. Systematic changes occur in the lattice parameters, polymorphic phase transition temperatures and dielectric properties below the Curie temperature for 0–2 h attrition milled powders and these are attributed primarily to an ion-size effect associated with Zr-doping on the Ti-site due to milling media contamination. The bulk conductivity of attrition milled samples at high temperature decreases by ~2–3 orders of magnitude compared to 0 h samples and the activation energy associated with bulk conduction increases from ~1 eV for 0 and 0.5 h samples to 1.4 eV for 3 h samples. The change in bulk conductivity and conduction mechanism for the attrition milled samples is attributed to aliovalent Y^{3+} dopant contamination from the milling media.

Keywords: Electrical properties; Electroceramics

1. Introduction

The structure–composition–property relationships of $BaTiO_3$-based ceramics have been widely investigated since the discovery of ferroelectricity in $BaTiO_3$ during the Second World War. The reasons for the interest are primarily two-fold. First, $BaTiO_3$-based materials offer a wide range of commercial applications, including dielectric materials for capacitors, positive temperature coefficient of resistance thermistors, memory devices, tunable microwave dielectrics, piezoelectrics and non-linear optics.[1] In this case, research is driven by the need to optimise or enhance a desired property (or figure of merit), often based on incremental changes in chemical composition, processing conditions, etc. to an existing product formulation. Second, $BaTiO_3$ is often perceived as a 'model' (non-Pb-based) ferroelectric perovskite-type oxide (ABO_3) which exhibits several polymorphic phase transitions and is therefore used to correlate important dielectric/ferroelectric properties such as variations in polymorphic phase transition temperatures, permittivity and dielectric loss with chemical doping and ceramic microstructure.

The influence of many isovalent dopants on the polymorphism and dielectric properties of $BaTiO_3$ have been studied in detail. For example, Zr-doping on the Ti-site ($BaTi_{1-x}Zr_xO_3$) is known to decrease the cubic to tetragonal phase transition temperature (T_c) in undoped $BaTiO_3$ from ~130 °C by ~5 °C/at.% Zr, however, it increases the transition temperatures associated with the subambient rhombohedral–orthorhombic ($T_{r/o} \sim -80$ °C) and near ambient orthorhombic–tetragonal ($T_{o/t} \sim +5$ °C) phase transitions by ~10 and ~4 °C/at.% Zr, respectively.[1–3] Zr-doping is often referred to as 'pinching' because the shift in phase transition temperatures with increasing x results in coalescence of all three transitions at ~50 °C for $x \sim 0.15$. In turn, this results in a single, broad permittivity peak at this temperature, as opposed to the three distinct permittivity peaks observed at −80, +5 and +130 °C for $x = 0$. For $x > 0.25$, relaxor-type ferroelectric behaviour is observed, viz. at temperatures below the maximum in permittivity, T_m, the real and imaginary parts of the permittivity (for a fixed temperature) decrease and increase with radio frequency, respectively. The

* Corresponding author. Tel.: +44 114 222 5974; fax: +44 114 222 5943.
E-mail address: d.c.sinclair@sheffield.ac.uk (D.C. Sinclair).

0955-2219/$ – see front matter © 2006 Published by Elsevier Ltd.
doi:10.1016/j.jeurceramsoc.2006.10.013

dielectric properties of $BaTiO_3$ are therefore extremely sensitive to Zr-doping and this is commonly exploited to broaden the temperature coefficient of capacitance in many $BaTiO_3$-based dielectrics for capacitor applications.

The defect chemistry and electrical properties associated with aliovalent doping of $BaTiO_3$ is a more complex subject and, in many cases, poorly understood. This is not surprising because charge compensation for a donor- (higher valent cation, e.g. La^{3+} for Ba^{2+}) or acceptor-dopant (lower valent cation, e.g. Ga^{3+} for Ti^{4+}) can occur by the creation of electronic and/or ionic defects. The situation is further complicated for dopants intermediate in size between Ba^{2+} and Ti^{4+} (e.g. Y^{3+}) as these can substitute on both lattice sites; therefore, depending on the Ba/Ti ratio of the starting composition can act as either a donor or an acceptor.

In general, acceptor doping results in the creation of oxygen vacancies, e.g. $BaTi_{1-x}Ga_xO_{3-x/2}$ and these materials exhibit good dielectric properties with no appreciable dc conductivity at room temperature. At elevated temperatures and modest pO_2 (e.g. ~1000 °C and 10–10^5 Pa), the isothermal dc conductivity exhibits p-type behaviour and therefore decreases with decreasing pO_2; however, for reducing atmospheres ($pO_2 < 10^{-10}$ Pa) n-type behaviour is observed and the isothermal dc conductivity increases with decreasing pO_2.[4] This variation in isothermal dc conductivity with pO_2 for acceptor-doped $BaTiO_3$ ceramics has been explained by Smyth and co-workers.[5] The p-type behaviour is attributed to filling of the anion vacancies ($V_o^{\bullet\bullet}$) with the creation of electronic holes ($h^{\bullet}$) by the following reaction:

$$V_o^{\bullet\bullet} + \tfrac{1}{2}O_2 \rightarrow O_o^x + 2h^{\bullet} \quad (1)$$

where O_o^x corresponds to oxide ions on their lattice sites. The n-type behaviour is attributed to oxygen loss with the creation of electrons (e') by the following reaction:

$$O_o^x \rightarrow \tfrac{1}{2}O_2 + V_o^{\bullet\bullet} + 2e' \quad (2)$$

This change in p- to n-type isothermal dc conductivity behaviour with decreasing pO_2 at elevated temperatures is also observed for undoped $BaTiO_3$ ceramics. Smyth and co-workers[5] attribute this unexpected p-type behaviour to unavoidable low levels (often <100 ppm) of acceptor impurities in the starting reagents used in preparation of $BaTiO_3$ powders, e.g. Fe^{3+} and Al^{3+} in TiO_2.

The dielectric properties of $BaTiO_3$ ceramics are also influenced by ceramic microstructure (i.e. average grain size and level of porosity)[6] and it is important to obtain suitably fine-grained and free flowing homogeneous powders prior to pressing green bodies and sintering to form dense ceramics. In most cases, powders prepared from the mixed oxide route are milled using either a ball mill or an attrition mill. The latter is a higher energy process and requires much shorter mixing periods and can usually produce finer powders compared to ball milling. In both cases, contamination from the milling media (usually some form of stabilized zirconia) is an unavoidable consequence of the need to produce appropriate powder for ceramic processing. Recently we have been investigating the influence of A- and B-site cation variance on the polymorphic phase transitions and dielectric properties of $BaTiO_3$ ceramics using isovalent dopants (A-site Sr, Ca and B-site Zr). Due to the refractory nature of the dopants we decided to investigate a two stage milling process, ball milling followed by a short period of attrition milling. This latter stage was used to further aid mixing and to reduce the average particle size of the powders prior to sintering. Given the sensitivity of electrical properties of $BaTiO_3$ to low levels of doping and the obvious concerns about contamination from milling we decided first to investigate the influence of attrition milling time on the electrical properties of undoped $BaTiO_3$ ceramics.

The work described here demonstrates that attrition milling of $BaTiO_3$ powder using yttria-stabilized zirconia (YSZ) milling media for short periods, e.g. 0.5 h has a small effect on the polymorphic phase transition temperatures and dielectric properties of undoped $BaTiO_3$ below T_c; however, it has a dramatic effect on the high temperature bulk conductivity. Attrition milling for >1 h results in significant changes to the polymorphic phase transition temperatures and for ~3 h development of core–shell microstructures and consequently significant changes in the dielectric properties below T_c and high temperature bulk conductivity mechanism. The changes in electrical behaviour are attributed to the influence of both iso- and alio-valent ion contamination from the milling media and serve as a 'cautionary tale' for the preparation of $BaTiO_3$ powders from high energy milling processes such as attrition milling.

2. Experimental

$BaTiO_3$ was prepared by conventional solid-state reaction of $BaCO_3$ (99.98%, Aldrich) and TiO_2 (99.9%, Aldrich). The raw materials in a 1:1 mole ratio (total weight ~30 g) were weighed and placed in a polypropylene bottle with propanol and magnesia stabilized zirconia balls and mixed for 12 h. The resulting slurry was dried in oven overnight before sieving through a 250 μm plastic mesh. The powder was placed in alumina crucible and calcined at 1100 °C for 6 h. The reacted powder was remilled as described above and re-calcined at 1150 °C for 12 h. In order to see the influence of different milling times (viz. 0.5, 1, 2 and 3 h) on the polymorphism and electrical properties of undoped $BaTiO_3$ ceramics, attrition milling was performed prior to sintering. In the present study we have chosen yttria-stabilized zirconia (ZrO_2-Y) balls as a grinding medium as the reported data suggests that ZrO_2-Y balls are less polluting than others such as agate. The experimental conditions fixed during attrition milling was; ball to powder ratio ~32 and the speed of stirrer ~300 rpm. Particle size analysis was performed using laser diffraction-based particle size analyzer (COULTER Electronics, LS130).

Pellets (10 mm diameter and ~1–2 mm thickness) were pressed at 200 MPa using a Cold Isostatic Press (Model CIP 32330, Cold Isostatic Press, Flow Autoclave System Inc., Columbus, OH). The green compacts were sintered in an oxygen atmosphere on Pt foil in two stages, firstly heated at 1450 °C for 1 h and then cooled down to 1300 °C and held for 4 h using a controlled heating and cooling rate of 5 °C/min. The density of the ceramics was determined using pellet dimensions and weight. Prior to microstructural analysis by scanning electron microscopy (SEM), pellet surfaces were polished using 1200

grit SiC emery paper followed by 6, 3 and 1 μm diamond paste. Samples were then thermally etched for 1 h at 100 °C lower than the sintering temperature and then gold coated to prevent surface charging in the microscope. Secondary electron images were obtained by SEM (Model MK II SEM, CamScan, Cambridge, UK) operating at 20 kV and a working distance of 1 cm. The purity of the reacted powder and phase formation was confirmed using X-ray diffraction (XRD), with a high resolution diffractometer (Cu Kα1, λ = 1.54059 Å, Model Stoe StadiP, Stoe and Cie GmbH, Darmstadt, Germany) operating in transmission mode. Data were collected using a position sensitive detector over a 2θ range 20–100° with a step size of 0.1° and count time of 45 s/step.

For transmission electron microscopy (TEM) pellets were mounted on a glass slide using a thermosensitive resin and ground to a thickness of ~20 μm. Copper rings of 3.05 mm in diameter with a 1000 μm circular hole were glued onto the ceramic foils using an epoxy resin. Samples were thinned until perforation using a Gatan Duo Mill ion beam thinner operated at an accelerating voltage of 6 kV with a combined gun current of 0.6 mA at an incidence angle of 15°. After perforation, the beam angle was reduced to 12.5° and thinning performed for 1/2 h. Samples were then carbon coated using a carbon sputtering unit (Model Emitech K950 carbon coater, Pfeiffer Vacuum, Asslar, Germany) and examined in bright-field mode using a TEM (Model EM 430, Phillips, Eindhoven, The Netherlands) operated at an accelerating voltage of 300 kV.

For electrical measurements (dielectric behaviour, impedance spectroscopy and hysteresis loops), electrodes were fabricated from gold paste (T-10112, Engelhard-CLAL, Cinderford, Gloucestershire, UK), which were fired in air at 800 °C for 2 h to decompose the paste and harden the residue. For impedance spectroscopy (IS) measurements, pellets were loaded into a conductivity jig and placed in a horizontal tube furnace controlled to ±1 °C. The data were recorded from room temperature to 700 °C in steps of 25 °C over the frequency range of 40 Hz to 1 MHz using an impedance analyzer (Model 4192A, Hewlett-Packard Co., Palo Alto, CA) and an applied voltage of 100 mV. All data were corrected for sample geometry and analyzed using the commercial software package Z-view (Version 2.1, Scribner Associates Inc., Charlottesville, VA). It was found unnecessary to correct the experimental data for stray impedances. The open-circuit "parallel" capacitance of the sample holder was only ~5 pF, whereas the corresponding value with the sample present was always much greater than ~500 pF. The lead impedance (<1 Ω) was always insignificant in comparison with sample impedances and could be ignored.

The dielectric properties were investigated over the frequency range 10^2–10^6 Hz using a precision LCR meter (Model HP 4284A, Hewlett-Packard, Palo Alto, CA) from room temperature to 300 °C. Low temperature dielectric measurements were conducted using closed cooling helium cryostat (Oxford Instruments Ltd., Oxfordshire, UK) with a temperature controller (Model No. ITC 503, Oxford Instruments Ltd., Oxfordshire, UK) accurate to ±1 °C. Measurements were performed over the frequency range of 40 Hz to 1 MHz using an Impedance Analyzer (Model 4192A, Hewlett Packard Co., Palo Alto, CA) and an applied voltage of 100 mV in the temperature range 10–300 K. Polarisation–electric field (P–E) hysteresis loops were recorded with a computer controlled modified Sawyer-Tower circuit supplied with sinusoidal electric field of 50 Hz.

3. Results

Room temperature (RT) XRD patterns for crushed powders of ceramics prepared from 0 to 2 h attrition milling time were single-phase and could be fully indexed as the tetragonal polymorph of $BaTiO_3$ using the space group *P*4*mm* and ICDD file 79-2265, Fig. 1(a). There is a significant and systematic change

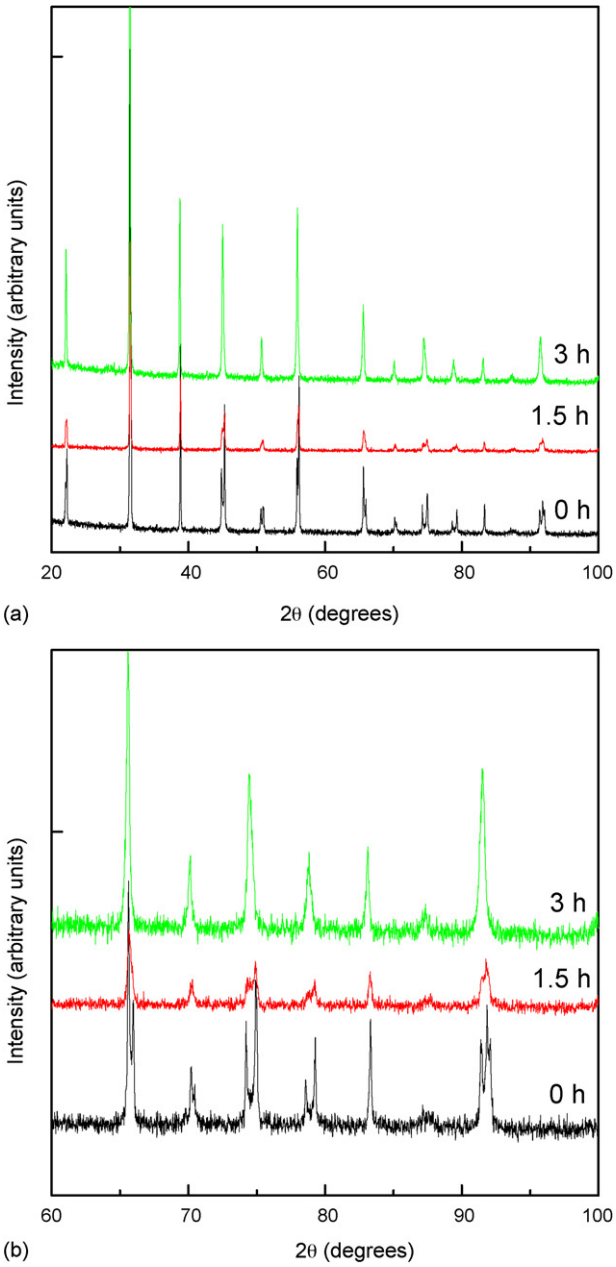

Fig. 1. (a) XRD patterns of crushed powders of ceramics prepared from various attrition milled powders and (b) expanded scale of the data for the 2θ range 60–100°.

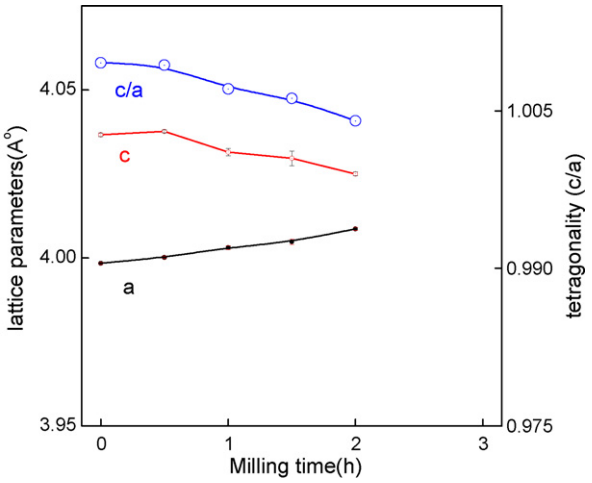

Fig. 2. Variation of a, c and tetragonality (c/a) of the powders at RT with attrition milling time.

in lattice parameters for these powders, with a increasing and c decreasing with milling time, Fig. 2. The c/a ratio clearly decreases with increasing attrition milling time. Although no extra reflections were observed in the XRD pattern for the 3 h milled powder, the data did not give a good fit to any one of the low temperature polymorphs (tetragonal, orthorhombic or rhombohedral cells) based on the ICDD data base. The difference for the 3 h powder is more clearly observed by inspection of XRD data at large two theta values, Fig. 1(b). The obvious peak splitting at ~75°, 79° and 91° 2θ for the 0 and 1.5 h samples is not present for the 3 h sample, instead the peaks are only slightly broadened. The lack of resolution in the diffraction data precludes an unambiguous assignment of the polymorphism and lattice parameters based on XRD for this sample.

Particle size distribution of the attrition milled powders prior to sintering of ceramics was measured using a Coulter particle size analyzer. Prior to attrition milling (0 h sample), d_{50} was ~1.2 μm, however, after 0.5 h attrition milling this reduced to ~0.7 μm. Further reduction in d_{50} was observed for 1 and 2 h milled powders, with values of ~0.5 and 0.4 μm, respectively. Milling for 3 h did not cause any further reduction in d_{50} which remained at ~0.4 μm. SEM micrographs of the ceramic microstructures obtained after sintering the various powders are shown in Fig. 3. There is a clear reduction in the average grain size of the ceramics prepared from attrition milled powders. For example, the 0 h sample has an average grain size of ~10 μm, Fig. 3(a), however, the grain size is smaller for the 0.5 h sample, Fig. 3(b), and is ~3 μm for the 2 h sample, Fig. 3(c). There appears to be a slight increase in average grain size for the 3 h sample, Fig. 3(d). These results are consistent with particle size distribution analysis of the powders, with the coarser powders resulting in larger-grained ceramic microstructures. In all cases, grain growth was limited during sintering and the lack of porosity, Fig. 3, is consistent with a measured pellet density of >95% of the theoretical X-ray density for all ceramics. In addition, EDS performed in the SEM showed clear evidence for the presence in some grains of (up to ~5 at.%) Zr-contamination in the 3 h sample.

The effects of prolonged attrition milling on the subgrain microstructure were examined by TEM. Bright-field images obtained for both the 0 and 3 h samples are shown in Fig. 4(a, b) and (c, d), respectively. The 0 h samples exhibit a variety of 90° ferroelectric domains that transverse the grains termi-

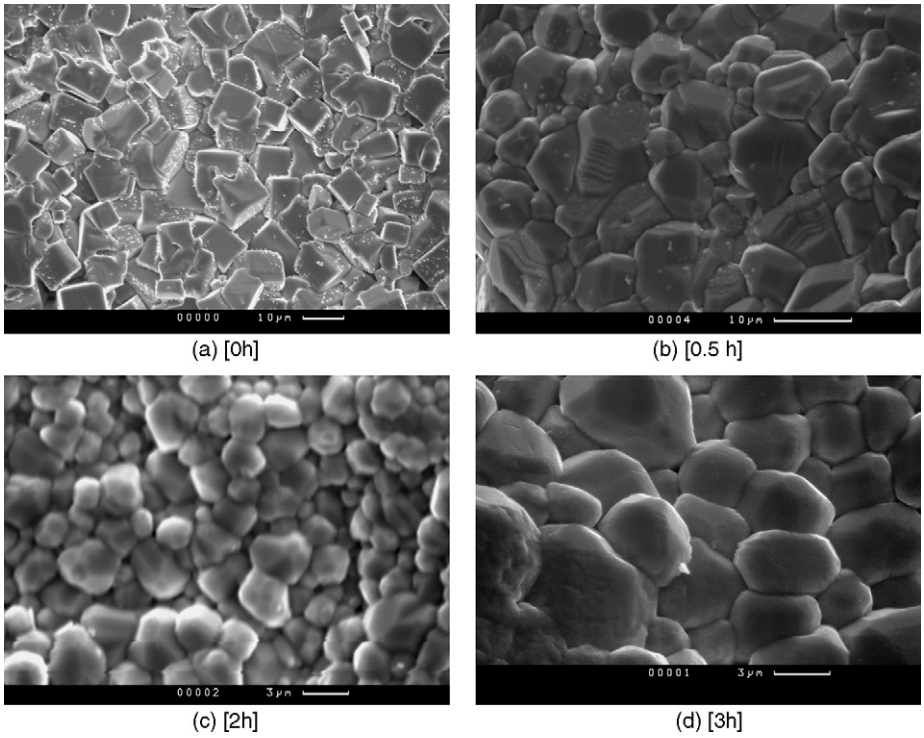

Fig. 3. SEM micrographs of sintered ceramics prepared from powders attrition milled for (a) 0 h, (b) 0.5 h, (c) 2 h and (d) 3 h.

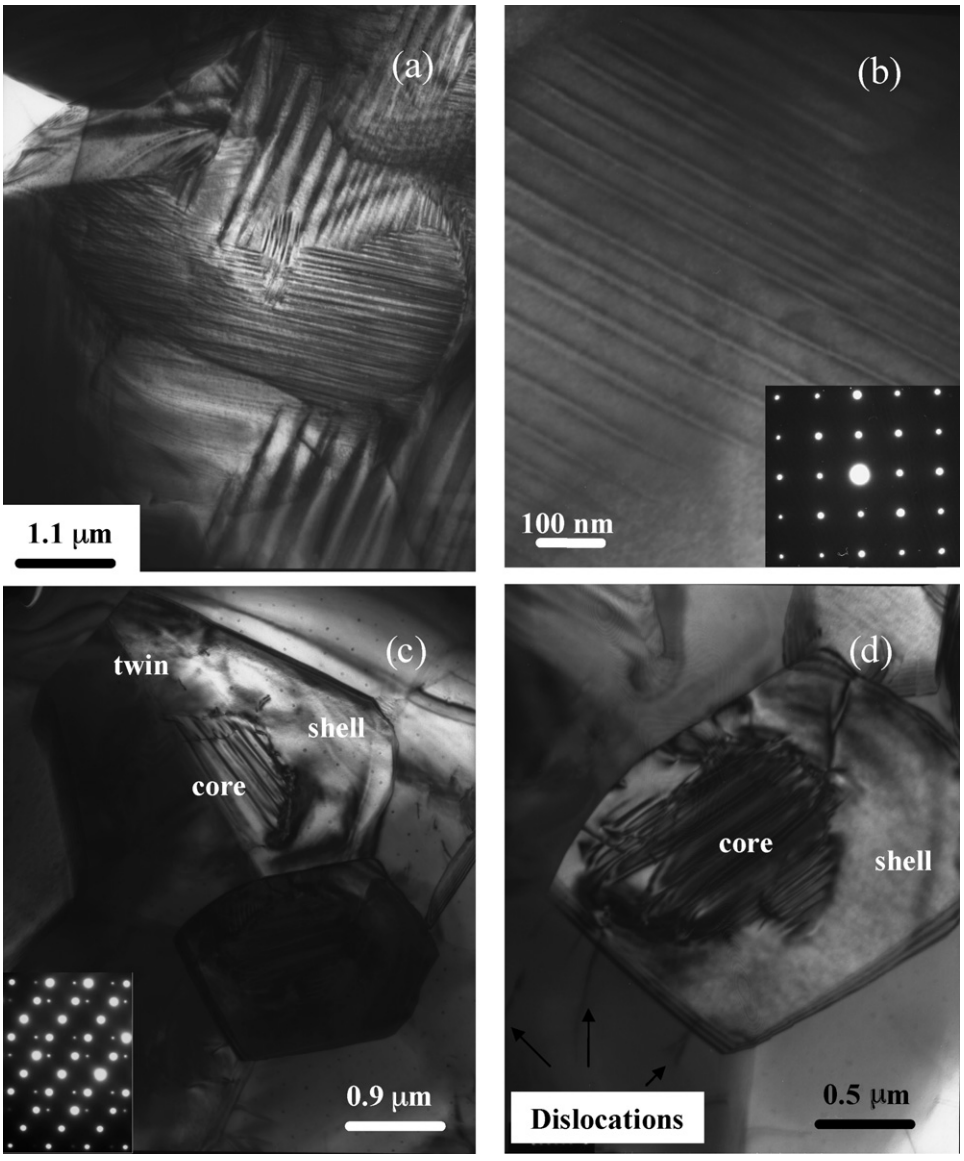

Fig. 4. Bright-field images for 0 h (a and b) and 3 h (c and d) samples. Insets in (b) and (c) show relevant electron diffraction patterns (see text for details).

nating at the grain boundaries, Fig. 4(a). Domain boundaries lie on {1 0 1} and domain widths vary between 20 and 80 nm, Fig. 4(b), which was obtained with the electron beam parallel to [1 0 0], as indicated by the inset diffraction pattern. Fig. 4(c) and (d) shows the typical subgrain microstructure observed for 3 h samples. Grains exhibiting a so-called 'core–shell' structure were often revealed. The core regions exhibit {1 0 1}-type twins, which is indicative that the core regions are ferroelectric, in contrast to the shell regions which are paraelectric. In general, core regions are ~1 μm in diameter and restricted to less than half the grain volume. Some grains exhibit twin interfaces, as illustrated in Fig. 4(c). The inset electron diffraction pattern obtained over the twin shows (1 1 1) to be the habit plane. This electron diffraction consists of two superposed [1 1 0]-type zone axes rotated by ~70°, which in this case can be readily identified by the different relative intensities of the reflections. The 3 h samples also exhibit a high population of dislocations, which in Fig. 4(c) appear as dots (more evident on the top right side of the figure), due to the orientation of the sample in relation to the electron beam. The dark grain in Fig. 4(c) imaged under a different orientation is illustrated in Fig. 4(d). A core–shell structure is revealed and under this orientation some dislocations appear as lines as indicated by the arrows.

The dielectric properties of ceramics prepared from the 0 and 0.5 h attrition milled powders are relatively similar with the exception of a decrease in T_c from ~130 to 126 °C, Fig. 5. Both exhibit a sharp maximum in permittivity at T_c, Fig. 5(a) and display similar subambient permittivity behaviour with clear evidence of permittivity peaks associated with the rhombohedral to orthorhombic and orthorhombic to tetragonal phase transitions with $T_{r/o}$ and $T_{o/t}$ being similar for both samples, Fig. 5(b). $\tan\delta$ is slightly higher between RT and ~100 °C for the 0 h sample, however, the general behaviour is similar with both samples exhibiting a peak in $\tan\delta$ at ~125–130 °C, Fig. 5(c). Ceramics from the 1–2 h milled powders display lower values of T_c compared to the 0 h sample and the associated permittivity

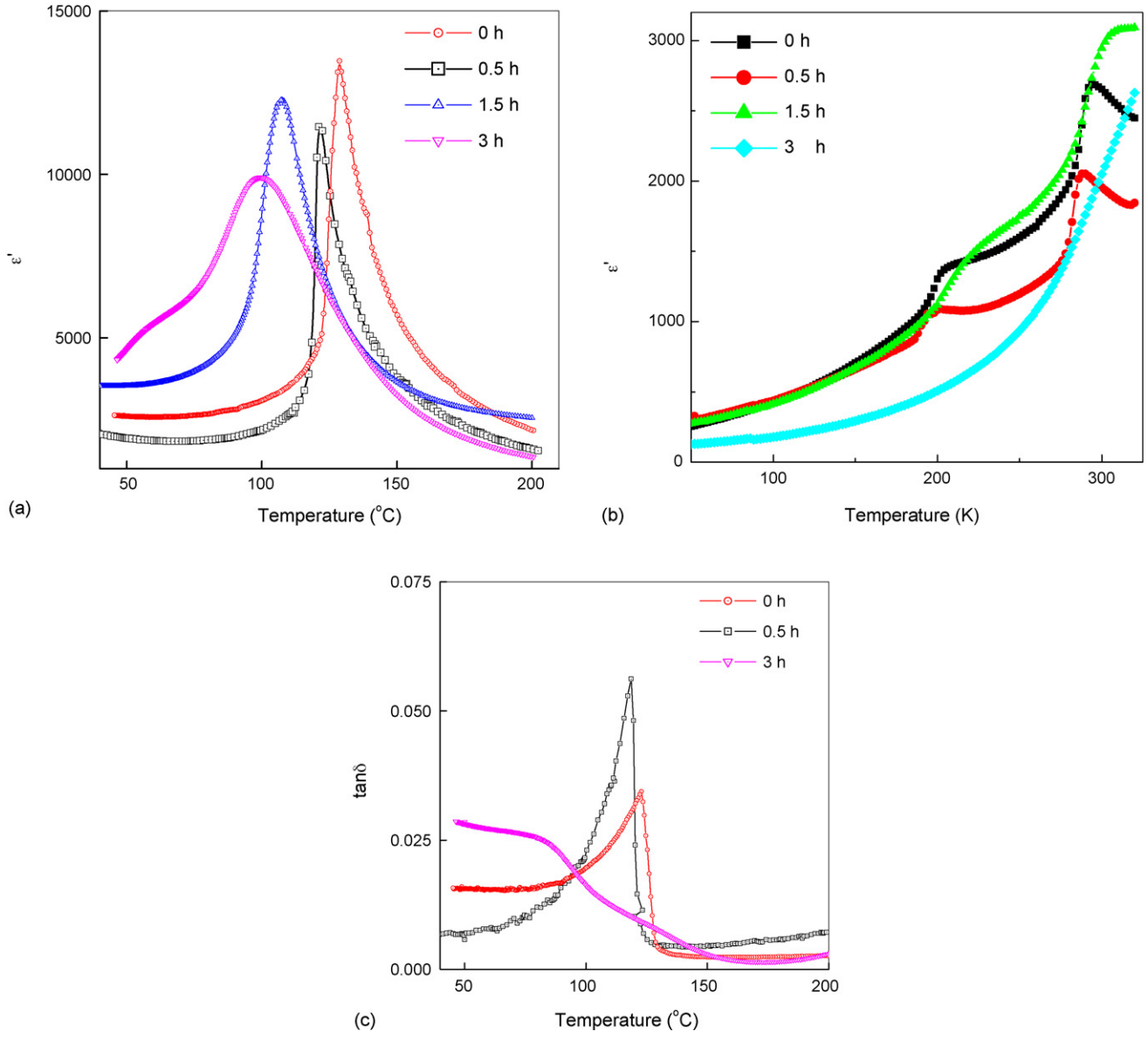

Fig. 5. Variation in permittivity (a) above and (b) below RT and (c) tan δ above RT for ceramics prepared from various attrition milled powders. All data collected at 1 kHz.

peak more rounded in shape, Fig. 5(a). Although the permittivity peaks below RT associated with the lower temperature polymorphic phase transitions are still discernable, $T_{r/o}$ and $T_{o/t}$ clearly occur at higher temperatures compared to the 0 and 0.5 h samples, Fig. 5(b). Although not shown, the loss behaviour for these samples are similar to that in Fig. 5(c) for the 0 and 0.5 h samples. In contrast, ceramics from the 3 h milled powders display very different dielectric properties, both above and below RT and as a function of frequency. No obvious peaks in permittivity are observed below RT, Fig. 5(b); instead two broad peaks in permittivity centred at ~60 and ~100 °C are observed, Fig. 5(a). In addition, tan δ does not show any peaks above RT; instead, the loss is initially quite high, ~0.03, but decreases with increasing temperature, exhibiting points of inflection at ~80, 110 and 135 °C. All samples exhibit similar loss values between 150 and 200 °C. The dielectric properties of ceramics prepared from 0 to 2 h milled powders did not exhibit any frequency dependence over the measured range 1–250 kHz. In contrast, ceramics prepared from 3 h milled powders displayed weak but significant frequency dependence indicative of ferroelectric relaxor-type behaviour, Fig. 6.

The permittivity peaks in the dielectric data were used to estimate T_c, $T_{o/t}$ and $T_{r/o}$ for ceramics prepared from 0 to 2 h milled powders and are summarised in Fig. 7. For 0–2 h samples, where sharp, well-separated peaks are observed, peak assignments to the various phase transition temperatures are unambiguous, however, this is not the case for ceramics prepared from 3 h milled powders, where only two permittivity peaks were observed. The assignment of these peaks will be discussed in detail later, however, based on the TEM results in Fig. 4(c) and (d) and the very different dielectric response for this sample, Fig. 6, it appears more appropriate to assign the

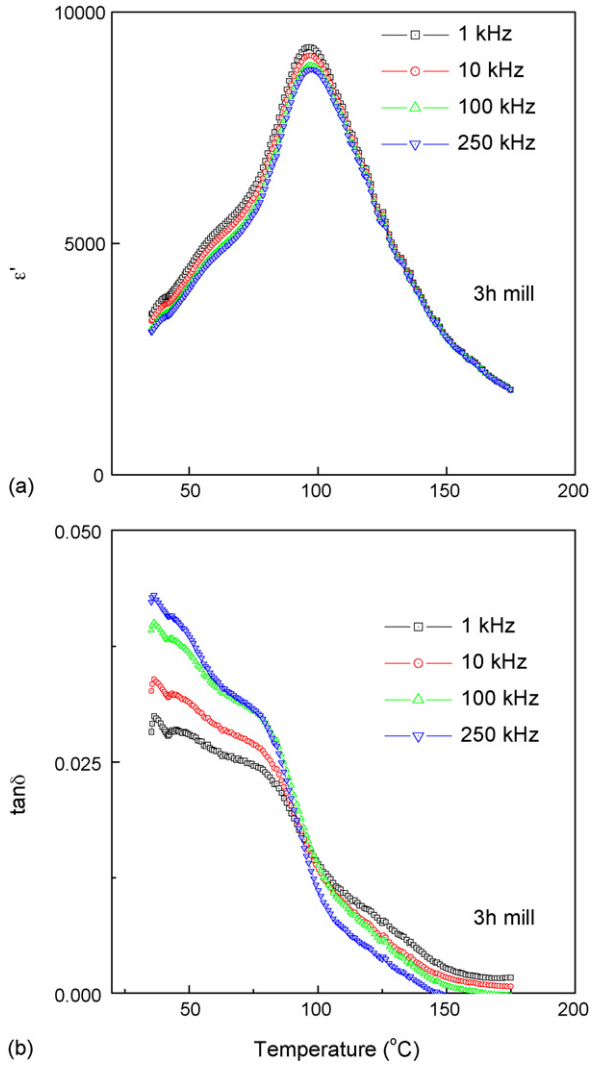

Fig. 6. Frequency dependence of permittivity and tan δ above RT for a ceramic prepared from a 3 h attrition milled powder.

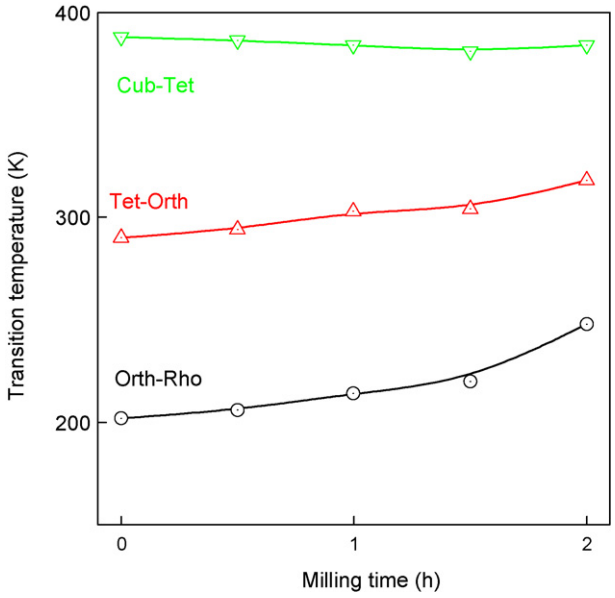

Fig. 7. Variation of $T_{t/o}$, $T_{o/t}$ and T_c for ceramics as a function of attrition milling time of the powder.

higher temperature peak to the ferro- to para-electric phase transition temperature associated with the core regions of the grains, whereas the lower peak at ~60 °C is associated with phase transitions in the shell-type regions of the subgrain microstructure.

Impedance spectroscopy (IS) was used to investigate the electrical homogeneity of the ceramics and typical complex impedance plane, Z^*, plots for data collected at ~500 °C for 0, 0.5 and 3 h samples are shown in Fig. 8. Two well resolved semicircular arcs are observed for ceramics prepared from 0 h attrition milled powders, Fig. 8(a). Based on an equivalent circuit consisting of two parallel RC elements connected in series, the low and high frequency arcs in the Z^* plot have associated capacitances of ~10 nF cm^{-1} and ~37.5 pF cm^{-1}. These are typical values for grain boundary (C_{gb}) and grain (bulk) responses (C_b) of ferroelectric $BaTiO_3$ ceramics in the paraelectric region based on the brickwork layer model for electroceramics and justify the choice of equivalent circuit to model the data.[7,8] Thus, the low frequency arc in Z^* plots can be attributed to the grain boundary response (R_{gb}, C_{gb}) and the high frequency arc is attributed to the grain response (R_b, C_b). Z^* plots for 0.5 and 3 h milled samples do not exhibit well resolved arcs, instead they consist of overlapping arcs. It was not possible to obtain reliable resistance and/or capacitance values from hand-fitting of the Z^* plots for these samples, however, the dc resistivity, R_T (where $R_T = R_b + R_{gb}$ based on the brickwork layer model) of the various ceramics was estimated from the low frequency intercept of the data with the Z'-axis. It is apparent from Fig. 8 that attrition milling of the powders causes a significant increase in the dc resistivity of the ceramics, increasing from ~60 kΩ cm for 0 h samples to >1 MΩ cm for the 0.5–3 h samples.

In an attempt to extract bulk and grain boundary R and C values from the IS data, analysis was performed using combined $-Z''$, M'' spectroscopic plots. This method can be used to estimate bulk and grain boundary R and C values for ceramics where there is significant overlap between the bulk and grain boundary arcs in Z^* plots. M'' spectra are dominated by the grain (bulk) response, and therefore the M'' Debye-type peak can be used to estimate R_b and C_b from the relationships $C_b = 1/2M''_{max}$ and $R_b = 1/(2\pi f_{max} C_b)$, where f_{max} is the frequency at the top of the M'' Debye peak. In contrast, Z'' spectra are dominated by the grain boundary response and therefore the Z'' Debye-type peak is used to calculate R_{gb} and C_{gb} using the relationships $R_{gb} = 2Z''_{max}$ and $C_{gb} = 1/(2\pi f_{max} C_{gb})$, where f_{max} is the frequency at the top of the Z'' Debye peak.[9] The combined $-Z''$, M'' spectroscopic plots at ~500 °C for 0, 0.5 and 3 h samples are shown in Fig. 9(a)–(c), respectively. Fig. 9(d) shows only the M'' spectra for the same samples and clearly shows f_{max} of the bulk M'' Debye peak to decrease dramatically from ~1 MHz for the 0 h sample to ~5 kHz for the 0.5 h sample. This demonstrates that R_b increases significantly for attrition milled powders, even for short milling times, e.g. 0.5 h. In addition, the M'' spectrum for the 3 h sample shows significant broadening with evidence of possibly two overlapping M'' peaks. This non-ideal Debye-like behaviour of the M'' spectrum demonstrates the bulk response for this ceramic to be electrically heterogeneous and is consis-

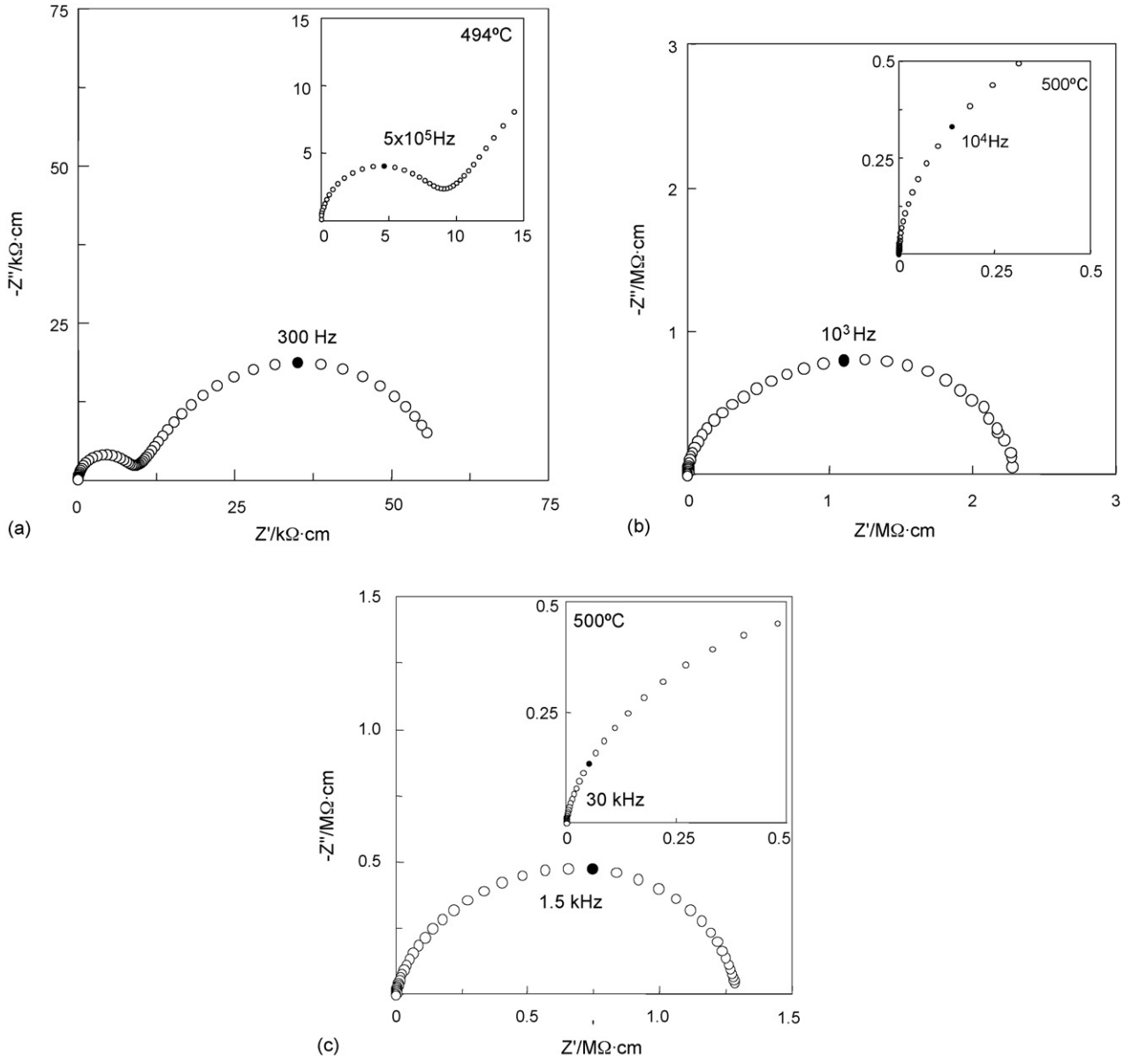

Fig. 8. Typical Z^* plots for ceramics prepared from (a) 0 h, (b) 0.5 h and (c) 3 h attrition milled powders.

tent with the core–shell microstructure observed from TEM in Fig. 4(c) and (d).

Arrhenius plots of the total conductivity, σ_T (where $\sigma_T = 1/R_T$ from Z^* plots), bulk conductivity, σ_b (where $\sigma_b = 1/R_b$ from the M'' spectra) and grain boundary conductivity, σ_{gb} (where $\sigma_{gb} = 1/R_{gb}$ from the $-Z''$ spectra) for various ceramics are shown in Fig. 10. All obey the Arrhenius law and therefore activation energies for the various conduction processes can be estimated from the slopes of these diagrams. σ_T, σ_b and σ_{gb} all decrease significantly for ceramics prepared from attrition milled powders, Fig. 10. It is particularly worth noting the increase in E_a for bulk conduction from ~1 eV for the 0 h sample to 1.4 eV for the 3 h sample, Fig. 10(b). Bulk and grain boundary conductivity data for a $BaZrO_3$ ceramic, BZ, (0 h powder) are included for comparison with the data for the $BaTiO_3$ ceramics, Fig. 10(b) and (c), respectively. The temperature dependence of C_b and C_{gb} are shown in Fig. 11(a) and (b), respectively. C_b decreases systematically with increasing temperature as expected for a ferroelectric material above its Curie temperature. C_{gb} displays weaker temperature dependence and it is noteworthy that C_{gb} for the 0 h sample is a factor of ~20 greater than the attrition milled samples.

The variation of σ_b at ~500 °C in flowing O_2 and N_2 atmospheres with time for 0 and 3 h samples is shown in Fig. 12. Although both samples exhibit p-type conductivity, the 0 h sample displays a larger variation in bulk conductivity with changing pO_2. Finally, P–E hysteresis loops for 1, 2 and 3 h samples are shown in Fig. 13. The coercive field, E_c and remnant polarisation, P_r are similar for all samples with $E_c \sim 1.4$ kV/cm and $P_r \sim 8.5$ μC/cm^2; however, the saturated polarisation, P_s is significantly lower for the 3 h sample with a value of 12 μC/cm^2

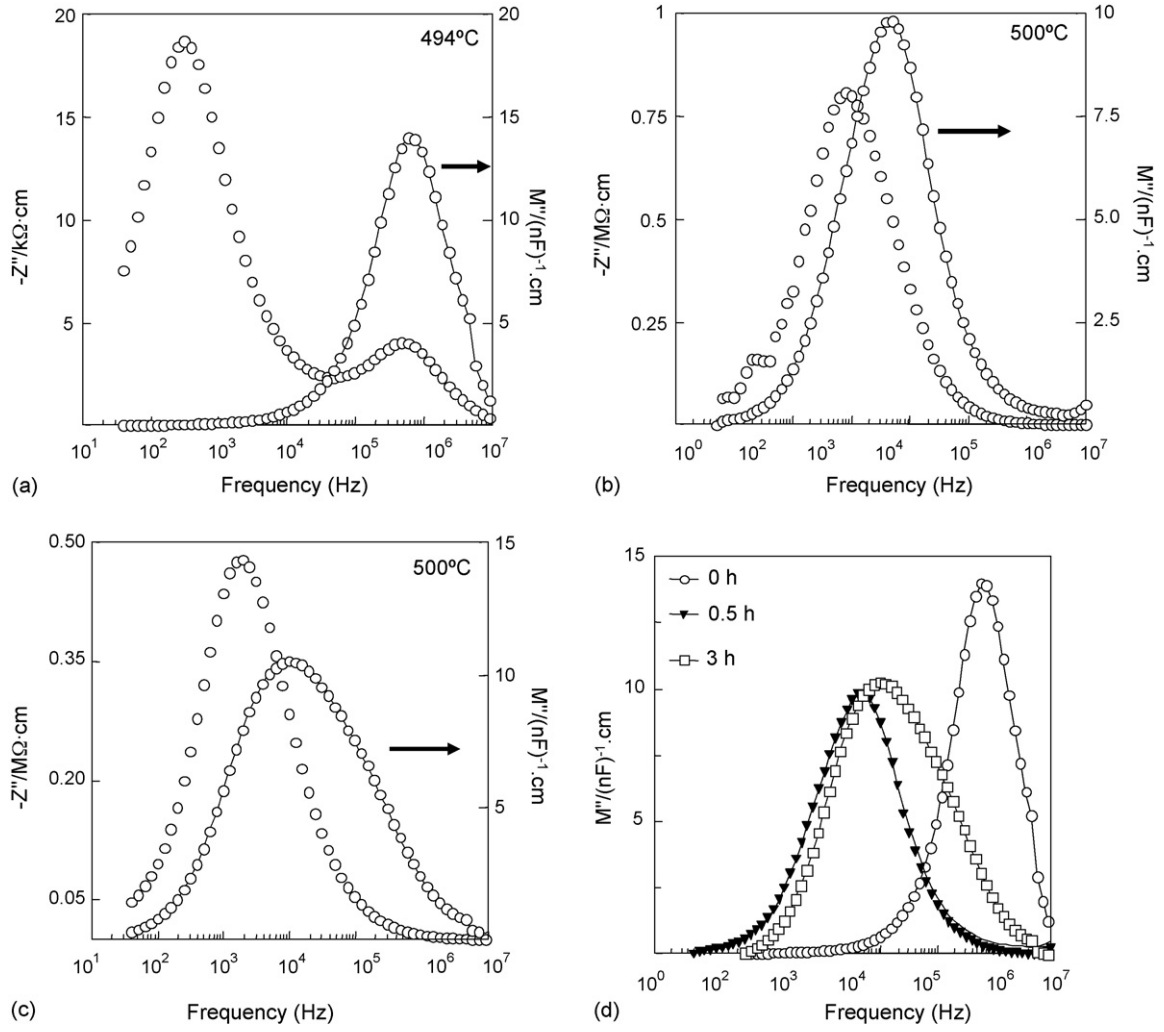

Fig. 9. Typical combined $-Z''$ and M'' spectroscopic plots for ceramics prepared from powders attrition milled for (a) 0 h, (b) 0.5 h and (c) 3 h, respectively. M'' spectroscopic plots for the same samples (d).

compared to 20 μC/cm^2 for the 1 and 2 h ceramics. Hysteresis loops for the 3 h milled sample are less square shaped than those for the other samples. This seems to indicate some degree of relaxor behaviour, as slim, inclined loops are typical for relaxor-type materials. The non-negligible dispersion of the permittivity (Fig. 6) supports the existence of relaxor character in 3 h samples.

4. Discussion

Attrition milling of $BaTiO_3$ powder using YSZ milling media has a significant effect on the dielectric and conduction properties of $BaTiO_3$ ceramics and is clearly related to unintentional contamination associated with the milling media. Attrition milling is a high energy process and therefore extended milling times are likely to lead to significant levels of contamination, as observed in the present study. In the case of $BaTiO_3$, where the electrical properties are extremely sensitive to the presence of low levels ($\ll$1 at.%) of dopants (intentional or unintentional), changes in composition can be detected by variations in lattice parameters, polymorphic phase transition temperatures, subgrain microstructure, dielectric behaviour <200 °C and/or electrical conductivity >300 °C.

Detection of Zr by EDS is the most direct evidence for Zr-contamination in the present study; however, reduction in tetragonality observed from XRD data, Figs. 1 and 2 and the general variation in polymorphic phase transition temperatures from the dielectric data, Figs. 5 and 7, are all consistent with that expected for the replacement of Ti^{4+} by the larger Zr^{4+} ion. The level of Zr-contamination in the 3 h sample was variable but was semi-quantitatively estimated to be as high as ~5 at.% in some grains from EDS using SEM. Based on an expected 5 °C/at.% Zr decrease of T_c for undoped $BaTiO_3$, the maximum in permittivity for the 3 h sample at ~100 °C, Fig. 6, is consistent with the level of Zr detected by EDS. The development of core–shell regions in some grains, Fig. 4(c) and (d), weak relaxor-type dielectric behaviour, Fig. 6, broad M'' spectroscopic plots from high temperature IS data, Fig. 9(c) and (d), and the lower P_s in the P–E hysteresis loops, Fig. 13, are all indicative of significant chemical heterogeneity in the 3 h sample. This may also explain why it was not possible to fit the XRD data of the 3 h sample to an indexing scheme based on a single polymorphic form of $BaTiO_3$.

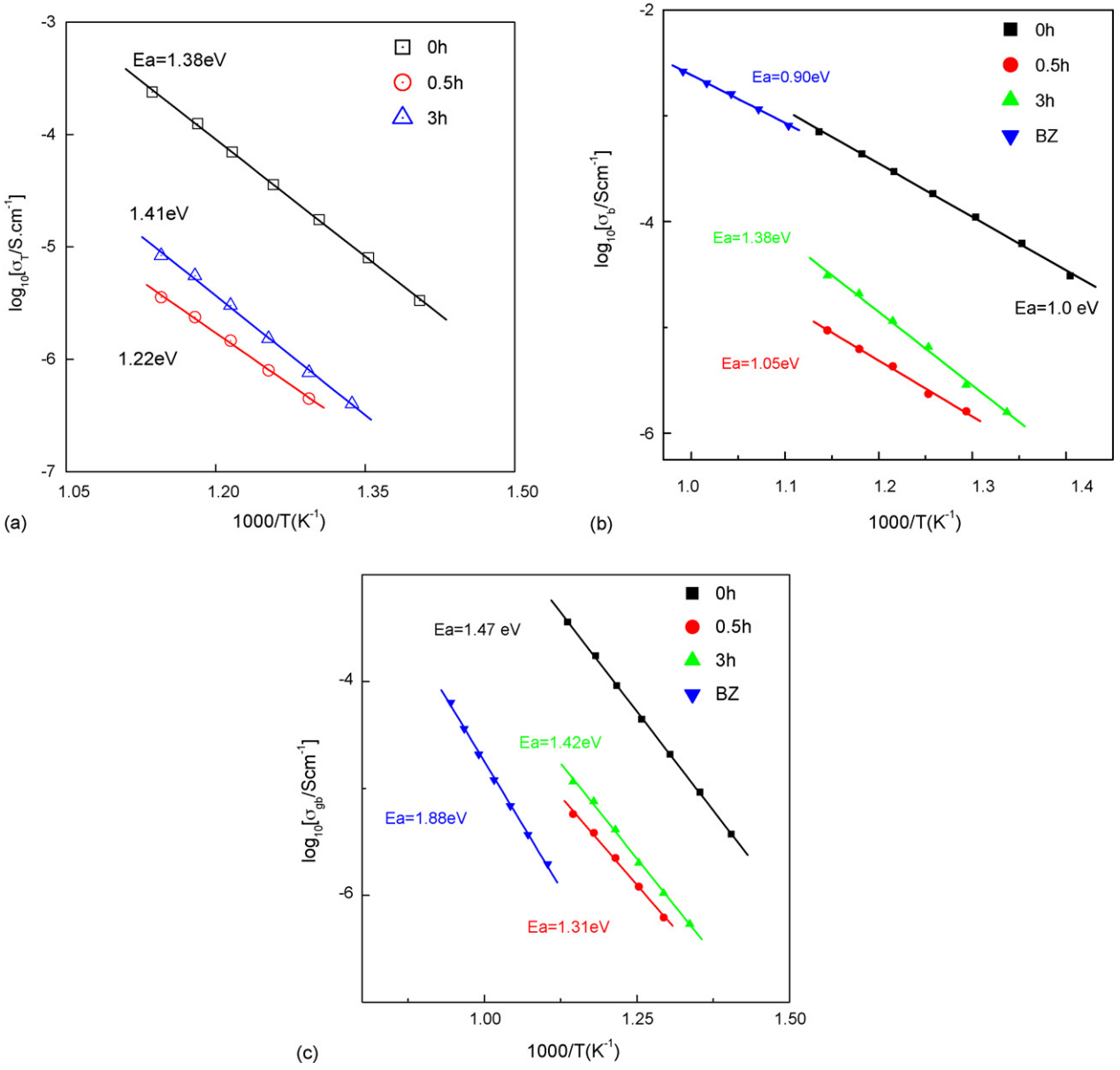

Fig. 10. Arrhenius plots of (a) σ_T, (b) σ_b and (c) σ_{gb} for ceramics from various attrition milled powders. BZ in (b) and (c) represents data from $BaZrO_3$ ceramics (0 h).

Core–shell subgrain microstructures and dislocations are commonly observed in doped-$BaTiO_3$ ceramics where incomplete diffusion of dopants is deliberately pursued. Different mechanisms have been suggested to explain the formation of core–shell structures in $BaTiO_3$-based materials[2,10] and although the exact mechanism responsible for their formation in the present study is not clear, it is most likely to arise from limited solid-state reaction between the $BaTiO_3$ particles with fine YSZ debris from the milling media. The higher level of contamination from YSZ debris for extended attrition milling periods is likely to result in the development of more core–shell type grains. This explains why they are more readily observed in TEM for the 3 h sample and also explains the significantly different dielectric response of this sample, viz. weak ferroelectric relaxor-type behaviour and the presence of only two 'peaks' in the permittivity data, Fig. 6 compared to the other samples, Fig. 5. Although the other attrition milled samples are likely to exhibit some core–shell structures, they are not sufficiently developed or widespread to dominate the dielectric properties and therefore the dielectric data from fixed frequency measurements of these ceramics reveal systematic changes in polymorphic phase transition temperatures as a function of milling time, Figs. 5 and 7.

It is also noteworthy that the average grain size does not change dramatically with attrition milling time, Fig. 3; however, it does scale with the average particle size of the starting powders. Since the grain size was >3 μm for all ceramics studied, there are no significant grain size effects, i.e. 'capping' of the fixed frequency permittivity data near T_c associated with a high volume fraction of grain boundaries due to a small (submicron) average grain size. TEM did reveal, however, significant

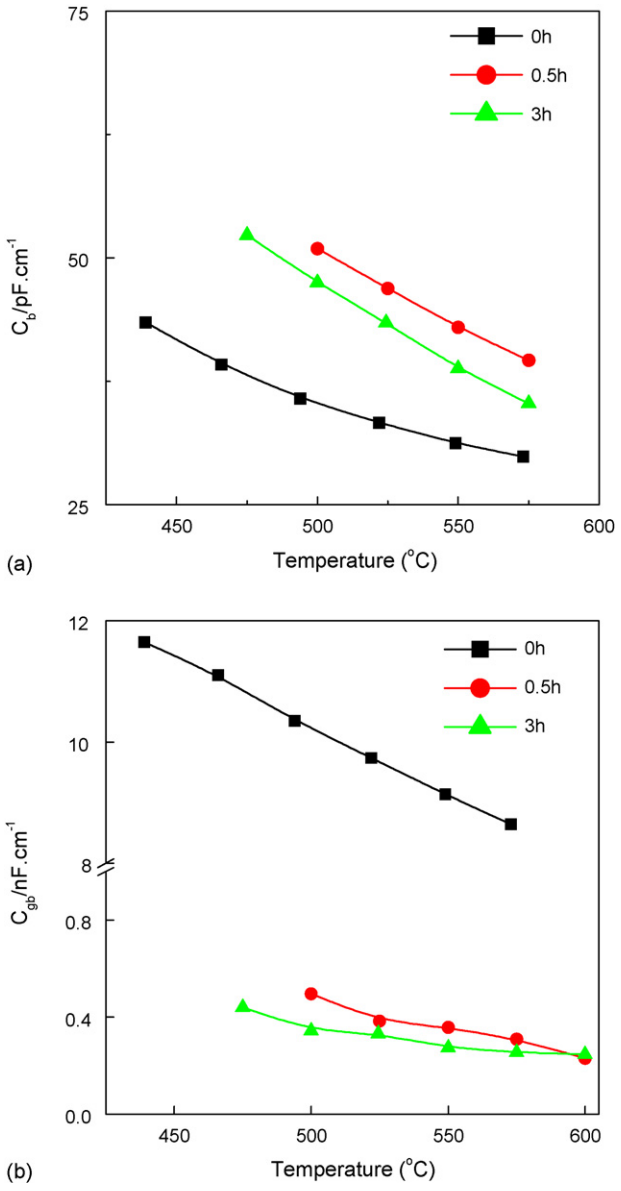

Fig. 11. Temperature dependence of C_b and C_{gb} for ceramics from various attrition milled powders.

differences in the subgrain structures of the 0 and 3 h samples. Although we do not wish to overinterpret the IS data, some comment on C_{gb} is required as it is at least one order of magnitude greater for the 0 h sample compared to the attrition milled samples, Fig. 11. Based on the validity of the brickwork layer model for the ceramics in this study, the higher capacitance associated with the grain boundary regions in the 0 h sample implies they are much thinner than that observed for the attrition milled samples. As the grain boundary response in undoped $BaTiO_3$ ceramics is normally attributed to space charge effects associated with dopant/defect segregation this region is narrow and well defined for ceramics from powder prepared by conventional ball milling. In contrast, the grain boundary regions for ceramics prepared from the attrition milled powders appear to be much thicker and may be related to the development of the core–shell microstructures associated with limited diffusion of

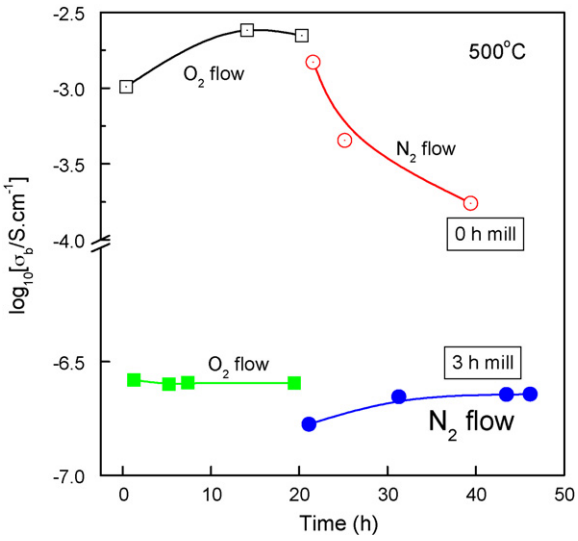

Fig. 12. Variation of σ_b with time at ~500 °C in flowing O_2 and then N_2 for ceramics prepared from 0 and 3 h attrition milled powders.

the contaminant ions. This general description is in reasonable agreement with the subgrain microstructures observed by TEM in Fig. 4, where 0 h samples exhibit a variety of 90° domains that transverse the grains and terminate at the grain boundaries, Fig. 4(a), whereas for 3 h samples, grains often exhibit core–shell structures whereby the core regions have an average diameter of ~1 μm and are normally restricted to less than half the grain volume.

In general, the dielectric behaviour of attrition milled samples can be explained on the basis of Zr-contamination from the milling media; however, there are several results pertaining to the high temperature conductivity studies that cannot be rationalized by isovalent substitution based on ion-size arguments. In particular, the dramatic change in σ_b and E_a of attrition milled samples, Figs. 9(d) and 10(b) and the rather weak pO_2 dependence of σ_b

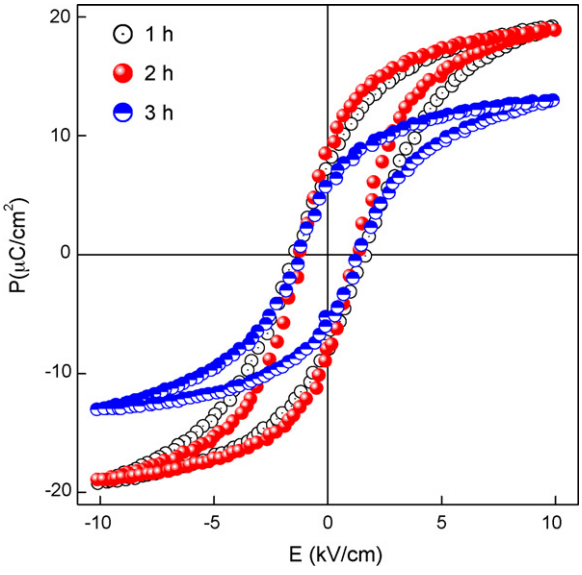

Fig. 13. Polarisation vs. electricfield hysteresis loops for ceramics prepared from various attrition milled powders.

for the 3 h sample, Fig. 12, require arguments based on aliovalent doping. For example, σ_b and E_a of ceramics prepared from ball milled $BaTiO_3$ and $BaZrO_3$ powders are shown in Fig. 10(b) and exhibit similar behaviour which can be explained by the 'extrinsic' acceptor-doped model for undoped powders as proposed by Smyth and co-workers[5] $E_a \sim 0.8$–1 eV is commonly quoted for the defect reaction given in Eq. (1) and this model also explains the strong dependence of the p-type bulk conductivity on pO_2, as shown for the 0 h sample in Fig. 12. Minor changes of lattice size associated with partial replacement of Ti^{4+} with Zr^{4+} will not influence the level of oxygen vacancies or the energy associated with this 'extrinsic' defect reaction.

The decrease in σ_b by ~3 orders of magnitude for the 0.5 h sample but E_a remaining at ~1 eV, Fig. 10(b), suggests the conduction mechanism remains 'extrinsic', as according to Eq. (1); however, some of the extrinsic oxygen vacancies initially present in the 0 h ball milled $BaTiO_3$ powder have been 'filled' and consequently there is a significant decrease in the bulk carrier concentration. A plausible explanation for this behaviour is aliovalent, donor-doping of (presumably) Y^{3+} on the Ba^{2+} site, according the mechanism, $Y^{3+} + (1/2)O^{2-} \rightarrow Ba^{2+}$. This requires only low levels of doping ($\ll$1 at.%) and provides an explanation for the dramatic decrease in σ_b for short attrition milling times. Although EDS did not detect the presence of any aliovalent impurities such as Y^{3+} in the ceramics they may be below the detection limit of the EDS system (~1 at.%).

Interpretation of the 'bulk' conductivity and the pO_2 dependence for the 3 h samples is limited because IS revealed the bulk response to be non-ideal, Fig. 9(d), and therefore electrically heterogeneous. Although the values of σ_b for the 3 h samples are subject to significant errors, the temperature dependence of σ_b (obtained from the variation of f_{max} from the M'' spectroscopic peaks) and therefore E_a associated with the bulk conduction can be obtained with reasonable certainty. Fig. 10(b) shows a significant increase in E_a from ~1 to 1.4 eV with increasing attrition milling time of the powders. The band gap, E_g of $BaTiO_3$ is ~3.0–3.2 eV and therefore, based on the assumption $E_a \sim E_g/2$, the activation energy for intrinsic conduction across the band gap is expected to be ~1.5–1.6 eV. The increase in E_a to ~1.4 eV (and the nearly pO_2-independent conductivity behaviour shown in Fig. 12) for the 3 h samples clearly suggests a change in bulk conduction mechanism. The 'extrinsic' acceptor-type model described in Eq. (1) is no longer valid, instead a more complex extrinsic model and/or a gradual switch-over towards 'intrinsic' conduction across the band gap seems more appropriate. In addition, gas–solid kinetics may be very slow for the 3 h sample due to the development of a significant core–shell microstructure.

Finally, in recent years there has been increasing interest in using high energy milling processes such as attrition milling for extended periods (often >100 h) as a 'low' temperature route to prepare a wide variety of mixed oxides.[11,12] Although these routes are often successful in preparing crystalline and nominally single-phase compounds, extended milling times inevitably result in significant levels of contamination and this may play an important role in the electrical properties of materials prepared by such methods. In the case of $BaTiO_3$, the influence of attrition milling, even for short periods of time, e.g. 0.5 h, has a significant effect on the electrical properties and we highlight this as a 'cautionary' note for other materials.

5. Conclusions

Contamination from YSZ milling media during attrition milling of $BaTiO_3$ powder has a significant effect on the electrical properties of undoped $BaTiO_3$ ceramics. The variation in lattice parameters, polymorphic phase transition temperatures and dielectric properties below T_c can be explained by unintentional Zr-doping on the Ti-site for powders attrition milled for $\leq$2 h. For longer milling times, e.g. 3 h, contamination induces significant levels of chemical heterogeneity such that a core–shell microstructure develops resulting in ferroelectric relaxor behaviour. Impedance spectroscopy shows the high temperature bulk conductivity to decrease by several orders of magnitude for ceramics prepared from $\geq$0.5 h attrition milled powders. In addition, the bulk conduction mechanism in ceramics prepared from ~3 h attrition milled powders deviates significantly from the well-established 'extrinsic' acceptor-doped model associated with oxygen vacancies, as given by Eq. (1). To explain the change in bulk conductivity and conduction mechanism it is proposed that unintentional donor-doping from the milling media (in this case Y^{3+} on the Ba-site) also occurs, albeit at a much lower level compared to the Zr-contamination. Although the defect chemistry of $BaTiO_3$ is a complex subject due to the wide range of chemical dopants and doping mechanisms that can occur, the sensitivity of its dielectric and conduction properties to low levels of iso- and alio-valent impurities make it an extremely effective material to study unintentional contamination associated with high energy mixing processes such as attrition milling.

Acknowledgements

We thank the EPSRC (OPT, AF and DCS) and the EU (BK) for financial support.

References

1. Jaffe, B., Cook, W. R. and Jaffe, H., *Piezoelectric Ceramics*. Academic Press, London, 1971.
2. Hennings, D. and Rosenstein, G., Temperature-stable dielectrics based on chemically inhomogeneous $BaTiO_3$. *J. Am. Ceram. Soc.*, 1984, **67**, 249–254.
3. Dobal, P. S., Dixit, A., Katiyar, R. S., Yu, Z., Guo, R. and Bhalla, A. S., Micro-Raman scattering and dielectric investigations of phase transition behavior in the $BaTiO_3$–$BaZrO_3$ system. *J. Appl. Phys.*, 2001, **89**, 8085–8091.
4. Rampling, M. J., Mather, G. C., Marques, F. M. B. and Sinclair, D. C., Electrical conductivity of hexagonal $Ba(Ti_{0.94}Ga_{0.06})O_{2.97}$ ceramics. *J. Eur. Ceram. Soc.*, 2003, **23**, 1911–1917.
5. Chan, N. H., Sharma, R. K. and Smyth, D. M., Non-stoichiometry in acceptor-doped $BaTiO_3$. *J. Am. Ceram. Soc.*, 1982, **65**, 167–170.
6. Arlt, G., Hennings, D. and Dewith, G., Dielectric-properties of fine-grained barium–titanate ceramics. *J. Appl. Phys.*, 1985, **58**, 1619–1625.
7. Sinclair, D. C. and West, A. R., Impedance and modulus spectroscopy of semiconducting $BaTiO_3$ showing positive temperature-coefficient of resistance. *J. Appl. Phys.*, 1989, **66**, 3850–3856.
8. Hirose, N. and West, A. R., Impedance spectroscopy of undoped $BaTiO_3$ ceramics. *J. Am. Ceram. Soc.*, 1996, **79**, 1633–1641.

9. Li, M., Feteira, A. and Sinclair, D. C., Origin of the high permittivity in $(La_{0.4}Ba_{0.4}Ca_{0.2})(Mn_{0.4}Ti_{0.6})O_3$ ceramics. *J. Appl. Phys.*, 2005, **98**.
10. Randall, C. A., Wang, S. F., Laubscher, D., Dougherty, J. P. and Huebner, W., Structure property relationships in core–shell $BaTiO_3$–LiF ceramics. *J. Mater. Res.*, 1993, **8**, 871–879.
11. van Hal, H. A. M., Groen, W. A., Maassen, S. and Keur, W. C., Mechanochemical synthesis of $BaTiO_3$, $Bi_{0.5}Na_{0.5}TiO_3$ and $Ba_2NaNb_5O_{15}$ dielectric ceramics. *J. Eur. Ceram. Soc.*, 2001, **21**, 1689–1692.
12. Stojanovic, B. D., Mechanochemical synthesis of ceramic powders with perovskite structure. *J. Mater. Process. Technol.*, 2003, **143**, 78–81.